# Electrocatalytic Oxygen Evolution on Iridium Oxide: Uncovering catalyst-substrate interactions and active Iridium oxide species

T. Reier[a], D. Teschner[b], T. Lunkenbein[b], A. Bergmann[a], S. Selve[c], R. Kraehnert[a], R. Schloegl[b] and P. Strasser[a]

[a] The Electrochemical Energy, Catalysis, and Materials Science Laboratory, Technical University Berlin, Department of Chemistry, Berlin, Germany
[b] Department of Inorganic Chemistry, Fritz-Haber-Institut der Max-Planck-Gesellschaft, D-14195 Berlin, Germany
[c] Zentraleinrichtung Elektronenmikroskopie, Technische Universität Berlin, D-10623 Berlin, Germany

## Abstract

The morphology, crystallinity, and chemical state of well-defined Ir oxide nanoscale thin-film catalysts prepared on Ti substrates at various calcination temperatures were investigated. Special emphasis was placed on the calcination temperature-dependent interaction between Ir oxide film and Ti substrate and its impact on the electrocatalytic oxygen evolution reaction (OER) activity. The Ir oxide films were characterized by scanning electron microscopy, transmission electron microscopy, scanning transmission electron microscopy, energy dispersive X-ray spectroscopy, X-ray diffraction, X-ray photoelectron spectroscopy and cyclic voltammetry. Furthermore, temperature programmed reduction (TPR) was applied to study the Ir oxide species formed as function of calcination temperature and its interaction with the Ti substrate. A previously unachieved correlation between the electrocatalytic OER activity and the nature and structural properties of the Ir oxide film was established. We find that the crystalline high temperature Ir oxide species is detrimental, whereas low temperature amorphous Ir oxy-hydroxides are highly active and efficient catalysts for OER. Moreover, at the highest applied calcination temperature (550°C), Ti oxides, originating from the substrate, strongly affect chemical state and electrocatalytic OER activity of the Ir oxide film.

## 1. Introduction

One major roadblock using renewable energy sources is an appropriate energy storage solution. Water electrolysis emerges as key technology for the long-term storage of energy. For this application proton exchange membrane (PEM) electrolyzers have the greatest potential due to low ohmic losses, low kinetic overpotentials and good partial load range achieved by the proton exchange membrane.(1) One of the biggest challenges connected with PEM electrolyzers is to provide improved anode catalysts (anode: oxidation of water to oxygen, oxygen evolution reaction OER) which offer high catalytic activity and stability against corrosion.(2)

With respect to the materials properties, Ir oxide is one of the best OER catalysts considering both activity and stability.(3) Therefore, Ir oxide constitutes, together with Ru oxide, the common active component in PEM anode catalysts.(1) Although Ir- and Ru oxide have been extensively studied during the past decades (3-10), the relationship between catalyst structure and composition on the one hand, and the OER reactivity on the other hand has remained unclear. Gottesfeld et. al. predicted, that the OER activity of Ir oxide decrease when changing from highly defective electrochemically prepared Ir oxides to stoichiometric $IrO_2$.(11)Therefore, amorphous catalysts tend to offer interesting electrocatalytic properties, but are often insufficiently characterized.

Conventional electrodes applied for the OER, like dimensionally stable anodes (DSA®), usually consist of thick porous layers having deep cracks.(12, 13) Ti is

commonly used as substrate and Ti oxide as inert matrix in which the active noble metal components, usually Ru- and Ir oxide, are dispersed.(14) Due to their complicated morphology, mass transport phenomena could restrict the catalytic process and impede kinetic analysis of DSA-type electrodes. Smooth, homogenous, thin-film catalyst layers prepared on the same Ti substrates constitute an adequate model system for conventional OER anodes. These thin-film catalysts allow excellent control over mass transport, offer a large surface area-to-bulk ratio, and good potential for the application of surface sensitive analytical techniques like X-ray photoelectron spectroscopy (XPS).

Previous works on substrate-supported OER film catalysts have grossly neglected a closer look at interactions of the substrate with the catalytically active coating. This is surprising, as the catalyst substrate junction is of great importance for the overall electrocatalytic activity of the catalyst system. For common OER catalyst systems utilizing Ti as substrate, several different catalyst substrate interactions appear plausible, for instance the catalyst can be chemically influenced by the substrate or an interlayer of a new compound can be formed at the junction between catalyst and substrate. This interlayer may have distinctly different electrocatalytic activity and/or electric conductivity. If the interlayer displays a poor electric conductivity, this can cause an additional voltage drop, resulting in the need for higher overpotentials, as recently demonstrated by Scheuermann et. al.(15). However, the characteristics of an interlayer formed during thermal preparation of Ru- or Ir oxide are not known. Also evidence was found by secondary ion mass spectroscopy that Ti is partly oxidized in this case,(16) the properties of this oxide layer and its impact on the OER remain unclear. Understanding and identifying materials at the catalyst substrate junction, their properties and their

interactions are therefore of great importance for rational catalyst design. Knowledge about the catalyst substrate interactions can contribute to pave the way to efficient, stable and inexpensive catalysts which are not available until now. Hereby, thin-film catalysts represent an adequate system for this investigation, since the catalyst-substrate junction, including a possible interlayer, constitutes a rather large fraction to the system, facilitating its investigation.

Here, we present a detailed study of amorphous and crystalline Ir oxide thin-film catalysts on Ti substrates, where we first follow the evolution of the chemical nature of the dominant Ir oxide species as function of the annealing temperature. We show how preparation conditions sensitively determine the OER activity of Ir oxide films. Particular emphasis is placed on the interactions of the Ir oxide film with the Ti substrate and how this interaction alters the Ir oxide properties. In the end, we achieve a correlation between the electrocatalytic OER activity of the Ir oxide films and their chemical state, but also take into account the influence of the substrate.

## 2. Experimental Section

Substrates. Three different substrates, Si wafers (<100>, B doped, Siegert Wafer), Ti coated silicon wafers (Ti/Si) and Ti cylinders, were used for the preparation of Ir oxide thin-films. Ti/Si's were prepared by physical vapor deposition of approximately 90 nm Ti onto the Si wafers. Ti cylinders (4 mm height, 10 mm diameter) were prepared by cutting Ti rods (Chempur, 99.7%). The cylinders were grinded and polished to a mirror like surface finish consecutively using SiC grinding paper, diamond suspension (9 μm, Buehler) and silica suspension (0.02 μm, Buehler) in a half automatic polishing machine (AutoMet 250, Buehler). Thereafter, Ti cylinders were treated in hot nitric acid (23%, prepared by dilution of 69% $HNO_3$, AnalaR Normapur) to remove surface impurities. Prior to spin coating all substrates were cleaned with ethanol and dried in nitrogen stream.

Film preparation. Thin precursor films were applied onto the substrate by spin coating (WS-650MZ-23NPP, Laurell). Standard substrate holders were used for Wafers, whereas custom made sample holders, providing a bigger coated surface area, were used for Ti cylinders to reduce boundary effects. To apply the coating, a 80 g $l^{-1}$ solution of Ir acetate (Chempur) in ethanol (abs., AnalaR Normapur) was applied onto the substrate rotating with 200 revolutions per minute (rpm) ensuring full coverage. Thereafter, the rotation velocity was increased to 2000 rpm with an acceleration of 200 revolutions $s^{-2}$ dwelling for 45 s to finish the spin coating process. Afterwards, the coated samples were calcined in a pre-heated Muffel furnace (Carbolite) at 250, 350, 450 or 550°C for 15 min.

Scanning electron microscopy (SEM). SEM images were acquired in secondary electron mode with a Jeol 7401F field emission SEM operated at 10 kV.

Scanning transmission electron microscopy (STEM) and transmission electron microscopy (TEM). S/TEM investigations were performed with a Cs corrected FEI Titan 80-300 equipped with an EDX detector (EDAX) and high angle annular dark filed (HAADF) detector. The sample was prepared in cross section along the <110> zone axis of the Si wafer. Therefore, two stripes were cut out of the wafer by a diamond wire saw. These two pieces were glued layer against layer and embedded by epoxy inside a Ti-grid. After the sample was grinded to a certain thickness, a dimple was polished to each side of the sample. As a final step the sample was ion-milled in a Fischione Ionmill Model 1010 under low incident angles and decreasing acceleration voltages, starting at 5 kV and 10° until finally 1 kV and 8°. Prior to measurements the sample was treated with Ar plasma for 30 s to remove severe contaminations.

X-ray diffraction (XRD). XRD profiles were measured in grazing incidence at 1° with Goebel mirror, Cu Kα source, a 0.23° secondary soller and scintillation counter as detector in a Bruker D8 Advance diffractometer (Bruker AXS) to increase the surface sensitivity. Data were collected with an increment of 0.05° and a measuring time of 40 s per step.

X-ray photoelectron spectroscopy (XPS). Ir oxide thin films on Ti coated Si wafers were characterized by X-ray photoelectron spectroscopy at the ISISS beamline of the synchrotron facility BESSY II of the Helmholtz-Zentrum Berlin. A detailed description

of the setup can be found elsewhere.(17) Samples were mounted onto a sapphire sample holder and introduced into the spectrometer. XPS experiments were carried out at room temperature in ultra-high vacuum (UHV).

Temperature programmed reduction (TPR). TPR was measured with coated silicon and Ti/Si substrates in a TPDRO 1100 (Thermo Fisher Scientific) from 30 to 600°C with a heating rate of 10 K $min^{-1}$ under 20 ml $min^{-1}$ $H_2$/Ar (4.05% $H_2$ in Ar, Air Liquide, purity 5N). Prior to TPR, the samples were dried in the same reactor at 125°C for 1 h under 20 ml $min^{-1}$ Ar (Air Liquide, purity 5N). The temperature inside the reactor at the sample position was measured by a type-K thermocouple sealed in a quartz capillary.

Electrochemical measurements. The electrochemical measurements were performed at room temperature in a rotating disk electrode (RDE) setup equipped with a three compartment electrochemical glass cell including a Luggin capillary, rotator (Pine research instrumentation) and a SP-200 potentiostat (BioLogic, France)(18, 19). A saturated mercury/mercury sulfate electrode was used as reference electrode. The reference electrode was calibrated against a reversible hydrogen electrode in the same electrolyte. All potentials provided in this article were converted and referred to the reversible hydrogen electrode. The electrolyte, 0.1 M $HClO_4$, was prepared by dilution of 70% perchloric acid (Sigma-Aldrich, 99.999%) with deionized water (18 MΩ cm at room temperature).

Electrochemical measurements were performed exclusively with IrOFs-coated Ti cylinders, which were mounted into custom-made PEEK sample holders. In the

electrochemical measurement, the samples were immersed at 1.200 V into the nitrogen degassed (15 min.) electrolyte, followed by three scans into the OER potential region. The first and third scan were measured with 6 mV $s^{-1}$ whereas the second scan was measured quasi-stationary with a potential step size of 20 mV, waiting 5 minutes at every applied potential for the current to equilibrate. In the quasi-stationary scan, impedance spectroscopy was carried out after every potential step to determine the ohmic resistance. After the three OER scans, the electrolyte was degassed with nitrogen (15 min.) holding the electrode at 1.200 V. Thereafter, cyclic voltammetry was measured between 0.400 and 1.400 V consecutively with the following scan rates: 500, 200, 100, 50 and 20 mV $s^{-1}$. 100 cycles were performed at 500 mV $s^{-1}$ to ensure a constant voltammogram, followed by 3 cycles at any other scan rate. Subsequently, the investigated voltage range was extended to reach from 0.050 to 1.400 V applying the same procedure as before. The OER measurements were performed with 1600 rpm RDE rotation speed while the cyclic voltammetry was measured with 0 rpm.

## 3. Results and Discussion

In this work, we explore the temperature dependent formation of chemically distinct Ir oxide species and show how they interact with a Ti substrate. In most previous OER studies, Ir chloride precursors were used for the thermal decomposition based preparation of Ir oxides (5, 20, 21). However, Ir chloride is known to decompose only partially at moderate temperatures leaving significant amounts of chloride impurities in the oxide film.(4, 22) Therefore, we used Ir acetate as chloride free precursor alternative to avoid chemical contaminations of the resulting Ir oxide film. Moreover, Ir acetate decomposes in air at moderate temperatures (T= 250 °C)(23) which allows us to study the properties of Ir oxide thin films calcined in a wide temperature range.

Thin Ir oxide films were coated onto a variety of different substrates (Ti cylinder, Si wafer and Ti coated Si wafer) to study the oxide films alone and their interaction with the Ti substrate. More specifically, polished Ti cylinders were used for electrochemical investigations since they can be measured under controlled mass transport conditions in a rotating disk electrode setup. To enable TPR studies and SEM cross section microscopy with a Ti substrate, Si wafers were coated with an approximately 90 nm thick Ti layer (labelled as Ti/Si). The Ti/Si substrate can be broken into pieces, which fit into the TPR reactor. Moreover, at the breaking edge cross section microscopy can be performed.

3.1. Morphology of Ir Oxide Thin-Film Catalysts

*3.1.1. SEM.* Figure 1 shows SEM images of Ir oxide films (IrOF) calcined at different temperatures. In the upper part of Figure 1 (a-d), top view images of IrOFs on Ti cylinders demonstrate that all films are homogeneous and smooth. The morphology changes as function of temperature. Starting at 250°C the film appears almost untextured. With increasing temperature the apparent porosity increases moderately. The apparent porosity can additionally be traced in the cross section micrographs applied on Ti/Si's (see Figure 1 e-h). The layered structure remains intact at all calcination temperatures but changes in morphology and layer thickness can be observed. The topmost layer is comprised of an approximately 55 nm thick Ir oxide layer. Underneath, between Ir oxide and Si wafer, the Ti layer can be observed with an approximate thickness of 90 nm. Interestingly, the Ti layer thickness is only constant up to 450°C. At 550°C this layer expands significantly to a thickness of about 140 nm and is converted into two distinguishable layers. In both layers the texture is increased compared to the Ti layer obtained at lower calcination temperatures. The upper layer consists of bigger grains. An expansion of the Ti layer under the applied conditions (calcination in air) can be rationalized by Ti oxide formation. If for instance Ti is oxidized to rutile type $TiO_2$, the unit cell expands from 35.7 Å³ to 62.5 Å ³(24). This would increase the former 90 nm Ti film to a $TiO_2$ film with a thickness of approximately 158 nm. Here, we observed only an increase to approximately 140 nm, demonstrating that either not the complete film is oxidized, as indicated by the observation of two differently textured layers, and/or that another Ti oxide species is formed.

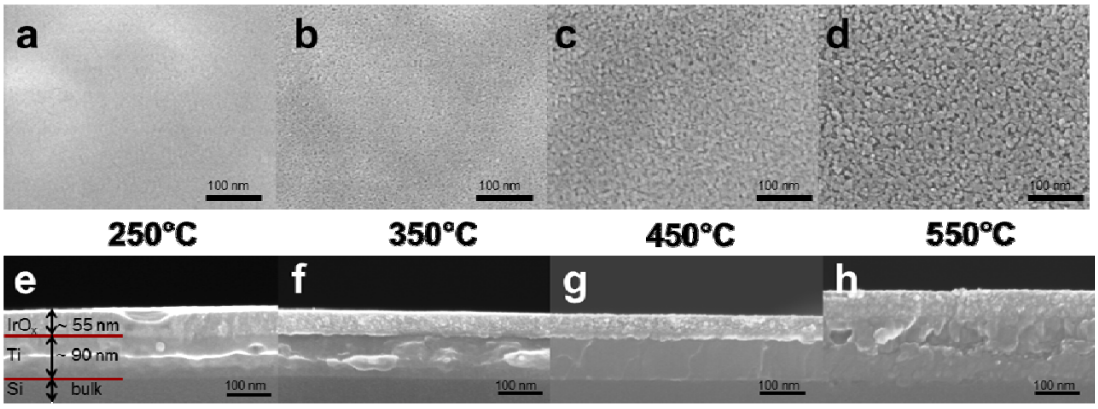


Figure 1. SEM images of Ir oxide films (IrOF) calcined at different temperatures. a-d: Topview images of coated Ti cylinders calcined at temperatures between 250°C and 550°C. e-h: Cross section images of IrOFs deposited onto Ti coated Si Wafers (Ti/Si) calcined at temperatures between 250°C and 550°C.

3.1.2. *TEM/STEM* A detailed analysis of the changes appearing at 550°C was performed on a thin electron beam transparent cross section of the IrOF coated Ti/Si by a combined analysis of TEM/HAADF-STEM measurements and EDX elemental mapping. (see Figure 2). The TEM and HAADF-STEM images (Figure 2a and b, respectively) demonstrate the existence of 4 different layers on top of the Si wafer, whereas only 3 layers where identified from the SEM image. Especially the layer L1 was not distinguishable in the SEM image (compare Figure 1h). The first approximately 17 nm thick layer (L1) is composed of Ti and Si as shown by the overlap of the corresponding EDX elemental maps(see Figure 2d and 2e) and could be most likely interpreted as formation of a titanium silicide. Only a small fraction of the Ti layer is mixed with silicon rendering the Ti in contact with Ir oxide uninfluenced by Si. Moreover, silicide formation

is retarded at lower temperatures resulting in even smaller amounts of silicide for all other calcination temperatures (25).

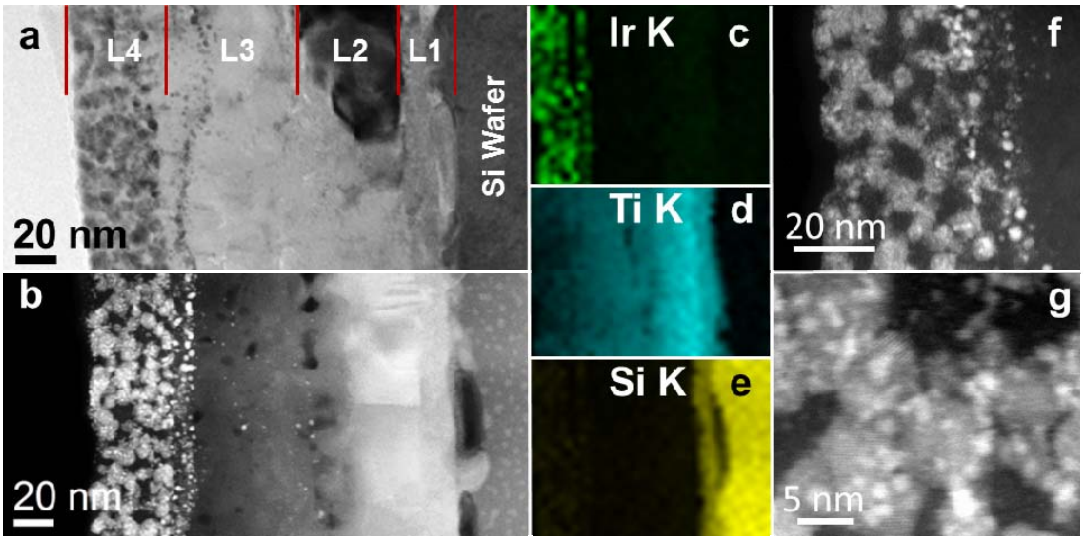


Figure 2: TEM/STEM cross section investigation of the Ir oxide film on a Ti coated Si wafer calcined at 550°C. a: TEM image (herein the 4 layers on top of the Ti/Si are labeled as L1-L4), b: corresponding STEM image, c-e: STEM-EDX elemental mapping over the layered system for Ir, Ti and Si with a lateral resolution of 5.5 nm, f: STEM image of the topmost layer (L4) and g: high resolution STEM image of L4.

The Ti and Si mixed layer L1 is followed by two mainly Ti containing layers L2 and L3. Considering the HAADF-STEM image (Figure 2b), wherein the contrast is due to Rutherford scattering approximately proportional to $Z^2$, layer L3 appears darker than layer L2. Under the given reaction conditions (calcination in air) this observation can most likely be explained by Ti oxide formation with an oxidation state gradient of Ti. Closer to the surface (L3) Ti is more oxidized, the oxidation state decreases deeper in the Ti bulk (L2). The top layer L4 constitutes the applied $IrO_x$ layer. An intermixing between L3 and the topmost layer L4 can be observed. The bright spots (see Figure 2b) within the

Ti oxide layer L3 indicate penetration of Ir oxide originating from layer L4. This interpretation is supported by EDX elemental mapping (see Figure 2c). Interestingly, Ti can also be found in layer L4 as demonstrated by EDX elemental mapping (see Figure 2d). In agreement with the HAADF-STEM images of layer L4 (Figure 2f and g) the obtained film after calcination at 550 °C consists of at least two different phases. In Figure 2g the bright regions correspond to Ir rich oxide species whereas the darker parts are due to a Ti rich species leading to morphology like a supported catalyst.

## 3.2. Structural Characterization of Ir Oxide Thin-Film Catalysts

3.2.1. *X-ray Diffraction.* Figure 3 depicts diffraction patterns of IrOFs on Ti cylinders calcined at different temperatures. The reflections at 250 °C can be assigned exclusively to the hexagonal phase of the Ti substrate (see Figure 3a) demonstrating that this Ir oxide film is X-ray amorphous, although the precursor has been decomposed at 250°C(23). An additional phase starts to grow at 350°C, identifiable by a small broad reflection at around 28° (see Figure 3b). This reflection grows in integral intensity and narrows with increasing calcination temperature, demonstrating the formation of a more crystalline phase with larger crystallite sizes. This phase can be identified as a rutile type oxide based on the additional reflections appearing at 450°C. Nevertheless at 550°C two rutile-type phases are discernible. Considering the materials applied, one rutile phase can be assigned to $IrO_2$, mainly due to the reflections at 34.7° and 40.1 discernible as shoulders of the Ti reflections at 35.1° and 40.2°, where $IrO_2$ reflections are separated from the $TiO_2$ rutile phase reflections. Rutile-type $TiO_2$ reflections, separated from $IrO_2$ reflections, appear at 36.1° and 41.2°, visible as shoulder of the Ti reflections at higher scattering angles. Nevertheless, since most reflections of the rutile-type oxides overlap and only

weak reflections are separated, a certain degree of intermixing cannot be excluded. At calcination temperatures of 450°C and 350°C reflections are too weak and too broad to decide if two rather similar or only one rutile phase is present.

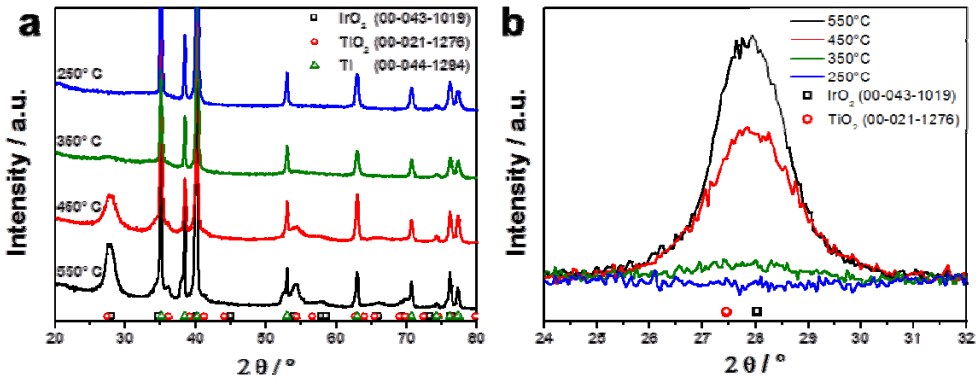


Figure 3 X-ray diffraction patterns of Ir oxide film coated Ti cylinders from 20° to 80° 2 Θ (a) and with linear background correction from 24° to 32° 2 Θ (b) to magnify the (110) reflection of the rutile type oxides. Reference patterns from the powder diffraction file (PDF) of the International Center of Diffraction Data are provided for comparison (reference number given in parentheses).

### 3.3. Surface Chemical Characterization

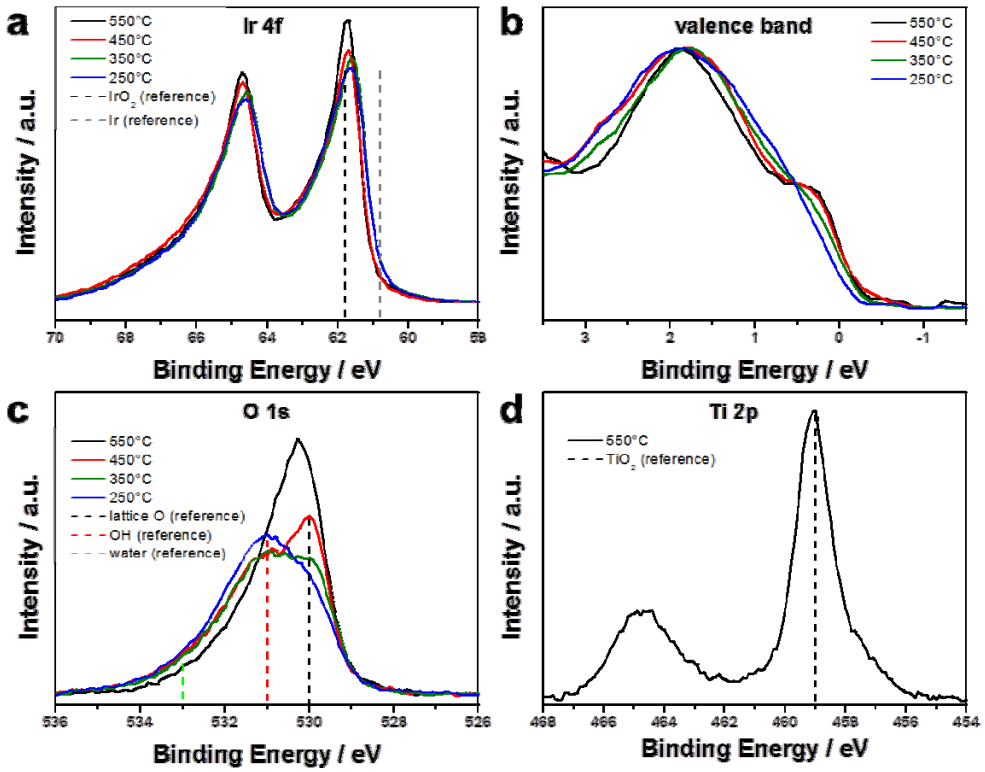


Figure 4. XPS measurements on Ir oxide films deposited on Ti coated Si wafers, (a) Ir4f region, (b) valence band, (c) O1s and (d) Ti2p region. Reference energies are provided for $IrO_2$ and Ir in Ir 4f, lattice O in oxide, OH and adsorbed water in O1s and $TiO_2$ in T2p. The applied photon energies were as follows. Ir4f and VB 599 eV, O1s 1080 eV and Ti2p 1010 eV.

3.3.1. *XPS.* The chemical state of near surface regions was characterized by X-ray photoelectron spectroscopy. Figure 4a shows photoelectron spectra of the Ir4f region of IrOF coated Ti/Sis for all calcination temperatures. The Ir4f region (Figure 4a) of all

samples shows an asymmetric peak profile, with the binding energy of ~61.7 eV, being very close to that of $IrO_2$. This demonstrates that oxidized Ir is present on all surfaces, even already after the lowest temperature of calcination. This is in line with Raman spectroscopic observations of Ir oxide prepared by calcination of Ir acetate at 250°C.(23) Closer inspection of the profiles reveals slight differences, as the spectrum of the 550°C calcined film is sharper and the width of the peak seems to increase towards lower calcination temperatures. The Ir4f spectrum after calcination at 550°C overlays perfectly with a reference $IrO_2$ sample measured in the same instrument.(26) The strong asymmetry of the $IrO_2$ signals is due to the high density of state at the Fermi level (Figure 4b) and a corresponding high degree of core hole screening (core hole- valence electron interaction).(27) The valence band reveals also a clear modulation of the density of states with calcination temperature. Lowering the calcination temperature decreases the occupation of low binding energy states. Owing to the direct coupling of the density of state and the Ir4f line shape, the small modulation of the Ir4f line shape has its origin in these differently occupied low binding energy states. The well developed Fermi edge of the films calcined at and above 450°C similar to $IrO_2$ indicates first neighbor Ir-Ir interactions. The valence band of the 250°C film suggests that the near surface region of the sample consists of an oxidized Ir, but the band structure typical for crystalline $IrO_2$ is not yet developed.

Figure 4c depicts the O1s spectra of the films with basically three components (adsorbed water: ~533 eV, hydroxyl groups: ~531-531.5 eV and lattice oxygen from $IrO_2$: ~530 eV) in varying ratios depending on the calcination temperature. All surfaces calcined between 250–450°C are predominantly hydroxyl terminated with a growing fraction of lattice oxygen upon higher calcination temperature. The lattice oxygen of

well-developed $IrO_2$ has similar asymmetric line shape, as observed for Ir4f.(27) However, due to the lack of crystalline $IrO_2$ phase after low calcination temperature, the asymmetrical line shape towards high binding energy suggests the presence of adsorbed water on all samples. At a calcination temperature of 550°C the spectrum of the O1s region changes drastically compared to lower calcination temperatures. Here, $TiO_2$ was detected in near surface regions with a Ti/Ir ratio of 0.9 (Figure 4d), but not upon lower calcination temperatures. Oxygen originating from Ti oxide overlaps with the other signals in the O1s spectrum after 550°C calcination. The appearance of Ti in the 550°C sample is in line with the observed intermixing of Ti oxide and Ir oxide (see Figure 2) and the morphological change (see Figure 1) exclusively found with this sample.

3.3.2. *Cyclic voltammetry.* Electrochemical surface characterization was performed by cyclic voltammetry as depicted in Figure 5. Figure 5a demonstrates large changes in the pseudo capacitive charge q*, recorded between 0.4 and 1.4 V, depending on calcination temperature. Remarkably, the charge q* decreases by more than one order of magnitude from the highest to the lowest temperature. The quantity of q* is frequently interpreted as a relative measure of the electrochemically active surface area (4, 20, 21), and therefore the decay of the pseudo capacitive charge has important implications for the intrinsic reactivity of the IrOFs. Compared to Ir oxide, Ti oxide has a small contribution to q*.(28) Hence, q* can be applied as good approximation for the electrochemically active Ir oxide surface area even in presence of Ti oxide. This is relevant for the IrOF calcined at 550°C where Ti oxide was identified in near surface regions. A surface area trend comparable to the q* values was observed within BET measurements of micelle-templated mesoporous Ir oxide films.(29)

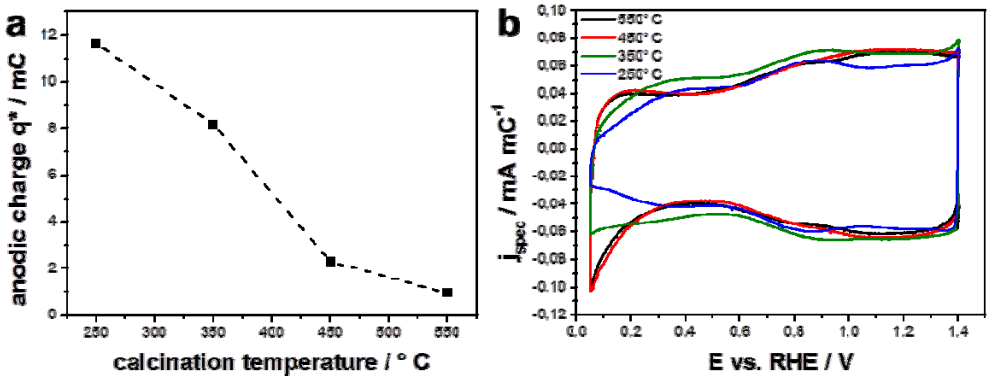


Figure 5. Anodic charge q* obtained by integration of anodic currents measured by cyclic voltammetry between 0.4 and 1.4 V (50 mV $s^{-1}$) for Ir oxide films on Ti cylinders (a). Cyclic voltammetry measured between 0.05 and 1.4 V with 50 mV $s^{-1}$ at room temperature in 0.1 M $HClO_4$ for Ir oxide films on Ti cylinders (b).

Figure 5b shows electrochemical surface redox properties of IrOFs calcined at different temperatures. Here, currents have been normalized with respect to q* (measured between 0.4 and 1.4 V, 50 mV $s^{-1}$) in order to provide comparable current densities. On the basis of this comparison, Figure 5b demonstrates different electrochemical redox properties for the films calcined at various temperatures. Samples calcined at 450°C and 550°C show significant current increase above 0.4 V leading to a plateau without formation of defined, clearly discernible peaks. This is a common behavior of thermally prepared $IrO_2$ electrodes (6, 21).

Notably, the IrOF calcined at 250°C shows a clearly distinguishable current peak at approximately 0.9 V. This peak is also present at 350°C calcination temperature, but is slightly shifted towards higher potential. The formation of such a peak is usually

observed for electrochemically formed Ir oxides, where it is connected to the $Ir(OH)_3/Ir(OH)_4$ redox couple.(3, 30) This implies a similar surface species to be present under the mild decomposition temperatures of 250 and 350°C.

Considering the low potential range in Figure 5b, further differences are evident. Samples calcined at 450°C and 550°C show a rather sharp reduction current close to 0 V lacking its direct counterpart in the anodic cycle, common for thermally prepared $IrO_2$ electrodes (6, 21). This feature is not observed for the IrOF calcined at 250°C. Here, the IrOF calcined at 350°C shows an intermediate behavior, not providing axial symmetry (with respect to the potential axis) like the 250°C sample, but neither displaying the sharp reduction current close to 0 V. Therefore, the 350°C IrOF can be regarded as intermediate state between the IrOFs calcined at 250°C and 450°C. Connecting this result to XRD and XPS measurements, we conclude that the surface chemistry of Ir oxide changes sensitively with crystallinity and the appearance of lattice oxygen at the surface.

### 3.4. Temperature programmed reduction: Ir oxide and its interaction with the Ti substrate

Temperature programmed reduction (TPR) probes the stability of oxides against reduction and is, therefore, highly sensitive towards their chemical properties. In a TPR measurement the sample is suited in a continuous $H_2$/Ar stream while the temperature is raised linearly. The hydrogen consumption is then measured as function of temperature, demonstrating which portion of the sample is reduced at which temperature. TPR is applied here to identify and analyze chemically different Ir oxide species and their interactions with the Ti substrate. Properties of pure Ir oxides, without interference of Ti

(oxides), were investigated utilizing silicon wafers as substrate. Control experiments by XRD (not shown) indicated no Ir silicide formation under the conditions applied here. Furthermore, uncoated but calcined (in air between 250 and 550°C) Si wafers were measured by TPR and showed no significant reduction peaks. Thus, for the TPR experiments we can rule out the interference of these two effects.

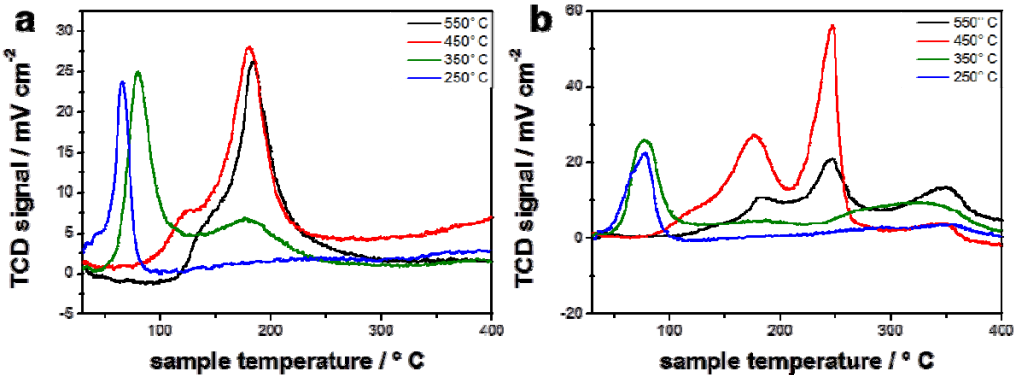


Figure 6. Temperature programmed reduction measured with 10 K $min^{-1}$. Ir oxide films on silicon wafers (a) and Ir oxide films on Ti coated Si wafers (b). The thermal conductivity detector (TCD) signal is normalized to the applied geometric film area.

Figure 6a shows TPR results for IrOFs on Si wafers. Here, significantly different reduction properties are apparent depended on the calcination temperature. The IrOF calcined at 250°C shows one major reduction peak around 70°C whereas the IrOF calcined at 550°C shows a major reduction feature at 180°C. This difference indicates a lower stability towards reduction for the IrOF calcined at 250°C.

The 550°C IrOF is not composed of only one Ir oxide species, as demonstrated by a small shoulder of the main peak around 150°C. This shoulder is more pronounced for the 450°C IrOF sample. However, beside this the TPR profile is similar to that at 550°C. Since IrOFs calcined at 450 and 550°C are crystalline whereas the 250°C IrOF is

amorphous, the observed difference in TPR can be correlated to the crystallinity of the IrOFs. Therefore, the main peak at 180°C can be attributed to the crystalline Ir oxide species and the peak at 70°C to the amorphous oxide/hydroxide. Interestingly, for the IrOF calcined at 350°C a mixture of both oxide types, the crystalline and the amorphous one, appears, with the larger fraction being the amorphous oxide. This result is in accordance with the intermediate behavior of the IrOF calcined at 350°C observed in cyclic voltammetry (see Figure 5b).

To probe interactions and chemical changes due to the presence of a Ti substrate, Ti/Si's were applied. Ti and Si are known to react at elevated temperature to form silicides (31). However, reference measurements with uncoated Ti/Si substrates revealed no TPR signals up to 400°C and therefore, if any Ti silicide formed, this does not interfere with the reduction pattern of the active coating.

TPR results reveal no significant differences between films on Si and Ti/Si calcined at 250°C (see Figure 6a and 6b). Thus, substrate oxidation effects can be ruled out at this temperature. For the 350°C sample the main features observed on Si are retained, but additionally a new very broad peak appears at approximately 320°C. Since the Ir oxide peaks are retained, this peak can be attributed to a Ti oxide. At 450°C the Ir oxide peaks observed on pure Si are retained in form and size, but additional peaks emerge at approximately 250°C and 350°C. Since Ir oxide is completely reduced at 250°C (signals from IrOF on Si fully retained), this peaks can be attributed to the reduction of Ti oxide species. The preservation of the Ir oxide signals indicate, that here Ir oxide is not chemically altered by Ti or Ti oxide. The 550°C sample displays some similarities to the

450°C sample. The peaks around 180°C, 250°C and 350°C are apparent. The latter two peaks have already been assigned to the reduction of Ti oxide species before. Compared to the film on pure Si, the main Ir oxide peak at 180°C diminishes. The diminishment of the Ir oxide peak demonstrates a partial chemical alteration of the Ir oxide species induced by the Ti substrate, maybe due to the formation of an Ir-Ti mixed oxide species. Evidence for this intermixing are obtained from STEM cross section microscopy (see section 3.1.2) and XPS (see section 3.3.1).

## 3.5. Electrocatalytic OER Activity

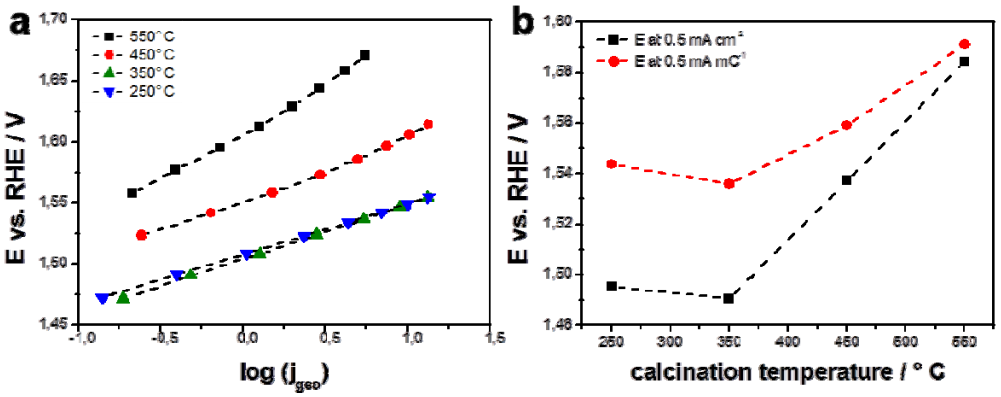


Figure 7. Quasi-stationary electrocatalytic oxygen evolution data measured on Ir oxide film coated Ti cylinders with 1600 rpm in 0.1 M $HClO_4$ at room temperature. The data were iR-corrected. Tafel plot (a) and the potential at a current density of 0.5 mA $cm^{-2}$ or respectively 0.5 mA $mC^{-1}$(b).

Figure 7a depicts Tafel plots of quasi-stationary electrocatalytic OER measurements and shows an almost identical OER performance for IrOFs calcined at 250 and 350°C. At higher calcination temperatures the curves are shifted towards larger potentials. The voltage necessary to reach a certain current density (0.5 mA $cm^{-2}$) can serve as measure

for the electrocatalytic OER activity of a catalyst and is depicted in Figure 7b. IrOFs calcined at 250° and 350°C provide the highest activity, while the activity drops at higher calcination temperatures. The IrOF calcined at 550°C requires the highest voltage and thereby offers the lowest activity. Hence, Ir is most efficiently used in the 250 and 350°C samples, since the Ir loading is constant for all films due to the applied spin coating process (compare Figure 1).

Due to the different calcination temperatures, the Ir oxide surface areas differ, as was shown in section 3.3.2. In Figure 7b, the influence of the Ir oxide surface area is excluded by normalizing the currents to q* (charge measured between 0.4 and 1.4 V, 50 mV $s^{-1}$). As pointed out before, q* is a relative measure of the electrochemically active surface area, thus this normalization results in intrinsic activities. Figure 7b depicts the potential required to reach a specific current density of 0.5 mA $mC^{-1}$ as a measure for the intrinsic OER activity. However, considering this measure the principle trend remains unchanged. The IrOFs calcined at 250 and 350°C remain the most active catalysts while the overpotential increases at higher calcination temperatures. Therefore, the observed differences in OER performance are at least partially of intrinsic nature (see Figure 7).

Tafel slopes in the range of 40 to 60 mV $dec^{-1}$ were observed for IrOFs calcined at and below 450°C, common for Ir oxides (5-7, 32). Notably, an unusually large Tafel slope of 72 mV $dec^{-1}$ was observed for the IrOF calcined at 550°C. As recently shown by Scheuermann et. al., introducing a $TiO_2$ layer between catalyst and substrate causes a sharp increase in OER potential and Tafel slope due to the poor conduction properties of $TiO_2$.(15) A Ti oxide interlayer was identified in the 550°C samples (see Figure 1 and 2),

which can explain the remarkably increased Tafel slope and additionally the lowest OER activity. However, the situation is somewhat more complex since indications for a chemical interaction between Ti- and Ir oxide were evident at 550°C (see section 3.1.2, 3.3.1 and 3.4). Remarkably, the observed difference in the OER activity between the IrOFs calcined at 350°C and 450°C cannot be explained on the basis of a Ti oxide interlayer, since the Tafel slope is not distinctly increased. Moreover, no indications for a chemical interaction between Ir oxide and Ti or Ti oxide were found at and below 450°C (compare section 3.4). Therefore, the observed difference in intrinsic electrocatalytic activity is related to the different Ir oxide present as function of calcination temperature. The amorphous oxy-hydroxide formed at low calcination temperatures provides a higher OER activity than the crystalline Ir oxide Hence, a higher structural flexibility seems to be beneficial for the OER performance together with the lower redox stability observed in TPR for the amorphous hydroxide.

## 4. Conclusions

We have explored the surface chemistry of Ir oxide thin-film catalysts on Ti substrates with special emphasis on the chemical and structural interaction of the Ti substrate with the catalytically active Ir oxide layer. We have identified two chemically distinct Ir oxide species, an amorphous and a crystalline species, that were formed as function of the applied calcination temperature. Electrocatalytic OER measurements demonstrated that the amorphous low temperature species provided a higher intrinsic OER activity than the crystalline high temperature species. Therefore, the best Ir utilization was achieved at

calcination temperatures of 250 and 350°C, which showed almost identical OER activities. Moreover, these moderate temperatures afforded maximum electrocatalytically active surface areas. Evidence for substrate (Ti) oxidation was detected from 350°C on. However, a severe impact of Ti oxide on the electrocatalytic OER activity was solely observed at 550°C. Here, a Ti oxide interlayer was formed and Ti oxide migrated into the Ir oxide layer. As a result the catalyst calcined at 550°C provided the lowest electrocatalytic OER activity.

## 5. Acknowledgments

We acknowledge Beatrice Kranzusch for the preparation of Ti coated Si wafers carried out in the laboratory of Dr. Bruns. Furthermore, we acknowledge the ZELMI for TEM sample preparation. This work was supported by the DFG Cluster of Excellence 'Unifying Concepts in Catalysis' and the DFG grant STR 596/3-1 as part of the Priority Program 1613 "Regeneratively formed fuels by light driven water splitting" which we both gratefully acknowledge.

## 6. References


1. M. Carmo, D. Fritz, J. Mergel and D. Stolten, *Int. J. Hydrogen Energy*, **38**, 4901 (2013).

2. H. Dau, C. Limberg, T. Reier, M. Risch, S. Roggan and P. Strasser, *ChemCatChem*, **2**, 724 (2010).

3. T. Reier, M. Oezaslan and P. Strasser, *ACS Catal.*, **2**, 1765 (2012).

4. S. Trasatti, *Electrochim. Acta*, **29**, 1503 (1984).

5. C. P. De Pauli and S. Trasatti, *J. Electroanal. Chem.*, **538-539**, 145 (2002).

6. S. Fierro, A. Kapałka and C. Comninellis, *Electrochem. Commun.*, **12**, 172 (2010).

7. L. Ouattara, S. Fierro, O. Frey, M. Koudelka and C. Comninellis, *J. Appl. Electrochem.*, **39**, 1361 (2009).

8. R. Forgie, G. Bugosh, K. C. Neyerlin, Z. Liu and P. Strasser, *Electrochem. Solid-State Lett.*, **13**, B36 (2010).

9. K. C. Neyerlin, G. Bugosh, R. Forgie, Z. Liu and P. Strasser, *J. Electrochem. Soc.*, **156**, B363 (2009).

10. E. Slavcheva, I. Radev, S. Bliznakov, G. Topalov, P. Andreev and E. Budevski, *Electrochim. Acta*, **52**, 3889 (2007).

11. S. Gottesfeld and S. Srinivasan, *J. Electroanal. Chem.*, **86**, 89 (1978).

12. A. R. Zeradjanina, F. L. Mantiab, J. Masa and W. Schuhmann, *Electrochim. Acta*, **82**, 408 (2012).

13. X. Wang, D. Tang and J. Zhou, *J. Alloys Compd.*, **430**, 60 (2007).

14. S. Trasatti, *Electrochim. Acta*, **45**, 2377 (2000).

15. A. G. Scheuermann, J. D. Prange, M. Gunji, C. E. D. Chidsey and P. C. McIntyre, *Energy Environ. Sci.*, **6**, 2487 (2013).

16. C. Piccirillo, S. Daolio, J. Kristóf, J. Mihály, B. Facchin and M. Fabrizio, *Int. J. Mass Spectrom. Ion Processes*, **161**, 141 (1997).

17. A. Knop-Gericke, E. Kleimenov, M. Hävecker, R. Blume, D. Teschner, S. Zafeiratos, R. Schlögl, V. I. Bukhtiyarov, V. V. Kaichev, I. P. Prosvirin, A. I. Nizovskii, H. Bluhm, A. Barinov, P. Dudin and M. Kiskinova, *Adv. Catal.*, **52**, 213 (2009).

18. T. P. Fellinger, F. Hasche, P. Strasser and M. Antonietti, *Journal of the American Chemical Society*, **134**, 4072 (2012).

19. M. Oezaslan, F. Hasché and P. Strasser, *Chemistry of Materials*, **23**, 2159 (2011).

20. L. A. da Silva, V. A. Alves, M. A. P. da Silva, S. Trasatti and J. F. C. Boodts, *Electrochim. Acta*, **42**, 271 (1997).

21. S. Ardizzone, A. Carugati and S. Trasatti, *J. Electroanal. Chem.*, **126**, 287 (1981).

22. G. Lodi, A. De Battisti, A. Benedetti, G. Fagherazzi and J. Kristof, *J. Electroanal. Chem. Interfacial Electrochem.*, **256**, 441 (1988).

23. T. Reier, I. Weidinger, P. Hildebrandt, R. Kraehnert and P. Strasser, *ECS Trans.*, **58**, 39 (2013).

24. Crystallographic Data on Minerals, in *CRC Handbook of chemistry and physics*, 90th ed., D. R. Lide Editor, CRC Press/Taylor and Francis, Boca Raton, FL (2010).

25. L. S. Hung, J. Gyulai, J. W. Mayer, S. S. Lau and M.-A. Nicolet, *J. Apply. Phys.*, **54**, 5076 (1983).

26. M. Moser, C. Mondelli, A. P. Amrute, A. Tazawa, D. Teschner, M. E. Schuster, A. Klein-Hoffman, N. López, T. Schmidt and J. Pérez-Ramírez, *ACS Catal.*, **3**, 2813 (2013).

27. G. K. Wertheim and H. J. Guggenheim, *Phys. Rev. B.*, **22**, 4680 (1980).

28. B. Johnson, F. Girgdies, G. Weinberg, D. Rosenthal, A. Knop-Gericke, R. Schlögl, T. Reier and P. Strasser, *J. Phys. Chem. C*, **117**, 25443 (2013).

29. E. Ortel, T. Reier, P. Strasser and R. Kraehnert, *Chem. Mater.*, **23**, 3201 (2011).

30. B. E. Conway and J. Mozota, *Electrochim. Acta*, **28**, 9 (1982).

31. S. P. Murarka and D. B. Fraser, *J. Apply. Phys.*, **51**, 342 (1980).

32. A. de Oliveira-sousa, M. A. S. da Silva, S. A. S. Machado, L. A. Avaca and P. de Lima-Neto, *Electrochim. Acta*, **45**, 4467 (2000).